Biophysical Journal Volume 107 November 2014 2230–2236

Article

Polarized THG Microscopy Identifies Compositionally Different Lipid Droplets in Mammalian Cells

Godofredo Bautista,[1,*] Simon G. Pfisterer,[2,3] Mikko J. Huttunen,[1,4] Sanjeev Ranjan,[2,3] Kristiina Kanerva,[2,3] Elina Ikonen,[2,3] and Martti Kauranen[1]

[1]Department of Physics, Tampere University of Technology, Tampere, Finland; [2]Institute of Biomedicine, Anatomy, University of Helsinki, Helsinki, Finland; [3]Minerva Foundation Institute for Medical Research, Helsinki, Finland; and [4]COMP Centre of Excellence and Department of Applied Physics, Aalto University, Aalto, Finland

ABSTRACT Cells store excess lipids as two major compounds, triacylglycerols (TAGs) and cholesteryl esters (CEs), inside lipid droplets (LDs). The degree of lipid ordering is considered to play a major role in the mobility and enzymatic processing of lipids in LDs. Here, we provide evidence that polarized third-harmonic generation (THG) microscopy distinguishes between native TAG- and CE-enriched LDs in cells due to the different ordering of the two lipid species. We first demonstrate that the responses from synthetic TAG- and CE-enriched LDs using THG microscopy with linear and circular polarizations differ according to their different intrinsic ordering. We then employ simulations to dissect how polarization effects influence the THG from an isotropic LD. Finally, we induce TAG- and CE-enriched LDs in murine macrophages and demonstrate that polarized THG responses increase in a nonlinear fashion with increasing CE/TAG ratio. This suggests that with an increasing CE content, there is a rather sharp transition toward increased LD ordering. Our results demonstrate that polarized THG microscopy enables label-free quantitative analysis of LD ordering and discriminates between compositionally different LDs in intact mammalian cells.

INTRODUCTION

Lipid droplets (LDs) are cytoplasmic organelles present in virtually all cells that typically range from hundreds of nanometers to several micrometers in diameter. They represent storage depots specialized for lipids, with the major lipid species being cholesteryl esters (CEs) and triacylglycerols (TAGs). The hydrophobic core of LDs is made up of CE and TAG surrounded by a phospholipid monolayer with associated regulatory proteins (1). Macrophages are important cells in the innate immune system, and CE and TAG deposition in macrophages play important roles in major health burdens: CE storage in macrophage LDs is a key process during atherosclerosis, the complications of which are a leading cause of death in western societies (2). TAG is stored in macrophage LDs, e.g., during *Mycobacterium tuberculosis* infection, which latently plagues one-third of the world population (3). Macrophage lipid storage also accompanies other prevailing epidemics, such as obesity (4) and fatty liver disease (5). At present, there is a clear need for improved detection of lipids and distinction between different lipid species at the cellular level.

The physical state of lipids, such as their structural order, affects their mobilization and enzymatic processing in LDs (6,7). At room temperature, or at human body temperature, TAG-enriched LDs are considered to be disordered with a fluid core, whereas CE-enriched LDs may display varying degrees of ordering, possibly even a crystalline state (7–9). A high degree of lipid ordering, typical, e.g., in atherosclerotic lesions (10), reduces CE clearance from LDs (11). It is therefore important to obtain generic information on lipid ordering in LDs. Traditional methods of determining LD ordering, such as differential scanning calorimetry, require cell disruption and extensive sample processing (12), which is not compatible with the analysis of intact cells or tissues. Conventional polarized light microscopy provides indications of the physical state of LDs but is not capable of 3D optical sectioning or of quantitative analysis (6).

Nonlinear optical microscopy techniques based on coherent anti-Stokes Raman scattering, second-harmonic generation (SHG) and third-harmonic generation (THG) are suited for label-free imaging of LDs (13,14) and lipid crystals (15) in cells and tissues. Coherent anti-Stokes Raman scattering is a spectroscopically resonant technique that can be used to visualize LDs, but the technique suffers from a nonresonant background and requires careful use of several laser sources (16). THG signals from biological samples derive from optical inhomogeneities (17) such as water and lipid interfaces, generating a high contrast from LDs (14). An additional advantage of THG is that it requires

Submitted February 24, 2014, and accepted for publication October 10, 2014.

*Correspondence: godofredo.bautista@tut.fi

Godofredo Bautista, Simon G. Pfisterer, Elina Ikonen and Martti Kauranen contributed equally to this work.

Editor: Katharina Gaus.

0006-3495/14/11/2230/7 $2.00

http://dx.doi.org/10.1016/j.bpj.2014.10.009

only a single laser source and thus is compatible with SHG and two-photon fluorescence imaging.

Moreover, because of its symmetry properties, THG microscopy with polarized light provides additional opportunities for visualizing LD ordering. In general, anisotropic domains are sensitive to the direction of linear polarization. This was recently employed to demonstrate that multilamellar model membranes exhibit ordering, whereas isotropic oil droplets in water do not exhibit significant ordering (18). On the other hand, THG signals for circular polarizations vanish in disordered (isotropic) materials regardless of their composition (19). In addition, differences in the response for left- and right-handed circular polarizations, i.e., circular-difference (CD) responses, can arise from oblique orientations of ordered domains (20), in accordance with the principles developed for SHG (21). Thus, nonvanishing THG signals for left- and right-handed circular polarizations, as well as differences between these signals, provide evidence of ordered domains (22).

In this article, we demonstrate that THG microscopy with linearly and circularly polarized input beams can be used to identify and discriminate between LDs of different lipid composition. We initially evaluate the capability of the technique by imaging synthetic TAG- and CE-enriched LDs with different intrinsic ordering. We then employ simulations to understand how polarization effects influence the THG responses from an isotropic LD. Finally, we apply the technique to a well-defined macrophage cell model with disease-related lipid depositions, showing its promise for simple and clinically relevant detection of lipid ordering at subcellular resolution.

MATERIALS AND METHODS

Cell culture

Raw 264.7 cells were cultured in growth medium (Dulbecco's modified Eagle's Medium (DMEM) supplemented with fetal bovine serum (10%), HEPES (10 mM), L-glutamine (2 mM), and penicillin/streptomycin (100 U ml^{-1} each)). Reagents for cell culture were from Life Technologies (Carlsbad, CA) or Lonza (Basel, Switzerland).

Generation of cellular CE- and TAG-enriched LDs, lipid determinations

Raw 264.7 cells were seeded in growth medium for 24 h, washed three times with phosphate-buffered saline, and incubated with control medium (DMEM supplemented with lipoprotein-deprived serum (5%)), with cholesterol/cyclodextrin complex (50 μM) or with oleic acid/bovine serum albumin (BSA; 400 μM) complex with Sandoz-58-035 (2 $\mu g\ mL^{-1}$) (an inhibitor of acyl-CoA:cholesterol acyltransferase 1, used here to inhibit CE incorporation into TAG-enriched LDs) in control medium for 24 h. Mixed LDs were generated by coadministration of 35 μM or 50 μM cholesterol/cyclodextrin and 400 μM oleic acid for 24 h. Cells were washed three times with phosphate-buffered saline and subjected to lipid extraction or fixed with paraformaldehyde (4%) for microscopy. For cellular CE and TAG determinations, lipids were extracted as described previously (23) using chloroform/methanol (1:1) and solvents were evaporated. Dried lipids were dissolved in chloroform/methanol (9:1) and resolved by thin-layer chromatography (TLC). TLC plates were charred, and cholesterol, TAG, and CE levels were quantified using ImageJ. Lipoprotein-deprived serum was obtained by potassium bromide density ultracentrifugation of fetal bovine serum (24). Oleic acid/BSA complex (8:1) was generated as previously described (25) using fatty-acid-free BSA. A methyl-β-cyclodextrin/cholesterol (6.2:1) complex stock solution (50 mM) was prepared according to the methods of Hsieh et al. (26). Methyl-β-cyclodextrin, fatty-acid-free BSA, cholesterol, and oleic acid were obtained from Sigma-Aldrich (St. Louis, MO).

Nonlinear microscopy

A custom-built transmission-mode nonlinear microscope powered by a mode-locked femtosecond Nd:glass laser (wavelength, 1060 nm; pulse length, 200 fs; repetition rate, 82 MHz; GLX-100, Time-Bandwidth, Zurich, Switzerland) was used in all THG experiments. After spatial filtering, collimation, and expansion, the laser beam was directed to an infinity-corrected and strain-free microscopy objective (NA 0.8). The objective was used to focus the beam onto the sample, which was mounted on a three-axis piezo-scanner (Thorlabs, Newton, NJ) controlled by LabVIEW. The transmitted unpolarized THG signal was collected by the condenser (NA 0.5), discriminated by suitable infrared blocking and interference filters (353 nm; Semrock, Rochester, NY), and detected by a cooled photomultiplier tube (PMC-100, Becker & Hickl, Berlin, Germany). A pixel dwell time of 100 ms was used in constructing the images. A transmission brightfield imaging arm was also incorporated to view the region of interest in the sample. To achieve controllable linear and circular polarization inputs, motorized half- and quarter-wave plates were used. Throughout the imaging experiments, average input power levels of 40 mW were used. All measurements were acquired at room temperature. Image analysis was performed using MATLAB and ImageJ.

RESULTS AND DISCUSSION

THG imaging of synthetic LDs

We first assessed the capabilities of polarized THG microscopy by using synthetic model systems for LDs that consisted of either pure TAG (glyceryl trioleate) molecules (TAG LDs) or mixed TAG and CE (cholesteryl linoleate) molecules in a 1:1 ratio (TAG/CE LDs). The samples were imaged with our THG microscope based on a femtosecond laser and tightly focused beams with linear and circular polarizations. We found that the synthetic LDs exhibited a strong THG signal well above the background (Fig. 1), in accordance with earlier findings (14). Using linear polarizations, we observed a strong polarization dependence of the THG signal, with a signal intensity for TAG/CE LDs ~17-fold higher than that for TAG LDs (Fig. 1, *a* and *b*). Application of left- and right-handed circular polarizations on synthetic LDs resulted in overall lower signal intensities compared to linear polarizations (Fig. 1, *a* and *b*). Interestingly, the THG signals from TAG/CE LDs were also relatively strong for circular polarizations, whereas the respective signals from TAG LDs were close to background (Fig. 1, *a* and *b*). These results suggest that TAG/CE LDs exhibit a higher level of ordering than pure TAG LDs.

To perform a more detailed analysis of LD ordering, we calculated the CD effects (THG-CD) for TAG and

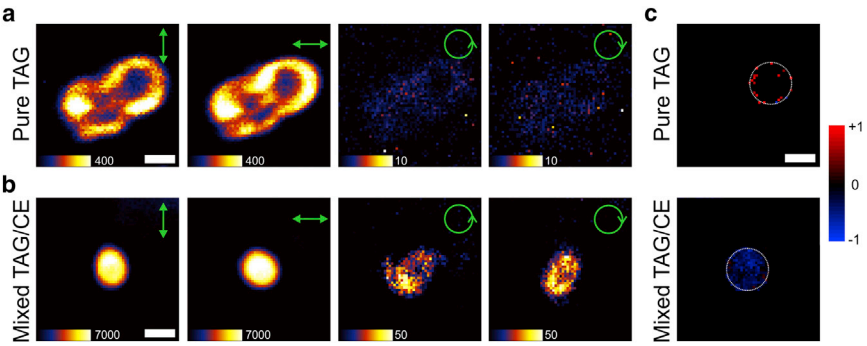

FIGURE 1 Polarized THG microscopy of synthetic LDs consisting of pure TAGs (*a*) and TAGs and CEs mixed at a 1:1 ratio (*b*) using orthogonal linear polarizations and opposite-handed circular polarizations at identical experimental settings. The direction of the incident polarization is shown by the arrow. Numbers at the lower left corner indicate the maximum signal level in each image. Scale bar, 2.5 μm. Images for TAG LDs represent a cluster of closely associated LDs. (*c*) Corresponding THG-CD images of the synthetic LDs. The THG-CD images were derived from the THG images using circular polarizations. The circle highlights the relative position of the imaged LD. For clarity, the spurious CD signals outside the highlighted region are not shown. Scale bar, 2.5 μm. To see this figure in color, go online.

TAG/CE LDs. THG-CD images were calculated using the equation

$$\text{THG} - \text{CD} = (I_{\text{RHCP}} - I_{\text{LHCP}})/[(I_{\text{RHCP}} + I_{\text{LHCP}})/2],$$

where I_{RHCP} and I_{LHCP} refer to the pixel intensity obtained using right- and left-handed circular polarizations. Whereas TAG LDs displayed very low THG-CD, mainly due to pixel-level noise, TAG/CE LDs gave rise to substantial THG-CD originating from the entire LD volume (Fig. 1 *c*). This further supports the notion that circular-polarization-dependent THG microscopy detects ordering in LDs.

All of the above results suggest that TAG/CE LDs exhibit a significant level of ordering, whereas TAG LDs are essentially disordered. Nevertheless, even TAG LDs exhibited polarization dependence in their THG response. More specifically, they gave a higher signal when the linear polarization was oriented along the local surface normal of the droplet than when it was oriented along the surface itself (Fig. 1 *a*). A simple interpretation might be that even TAG LDs exhibit local ordering at the LD-water interface.

THG modeling of an isotropic LD

To better understand the principles underlying the above results, we performed numerical simulations of the experiment (see Supporting Material for full details). Our simulations were based on calculating the far-field THG response of an isotropic LD near a tightly focused vectorial excitation field provided by the microscope objective (Fig. 2) (27,28). Under focused linear polarizations, the simulated THG signals from the LD resulted in a doughnut-like appearance (Fig. 2 *a*). In addition, the THG signals for linear polarization were maximal if the local surface normal of the LD was parallel to the direction of the incident linear polarization and minimal if it was perpendicular (Fig. 2 *c*). Among the wide range of simulations we have performed, we did not find any deviations from this rule, although the difference between the maximum and minimum varies. This is very similar to the experimental findings for TAG LDs (Fig. 1 *a*). The experimental results on linear polarization (Fig. 1 *a*) are therefore not an indication of local ordering at the LD-water interface. Instead, they arise naturally for an isotropic droplet when the polarized focal fields are properly taken into account. This finding shows that contrary to current thinking, the dependence of THG on linear polarization does not necessarily imply an anisotropic sample.

On the other hand, the simulations predicted that tightly focused circular polarizations produce weak THG signals (Fig. 2 *b*). Note that here also the signal arises from the vectorial character of the focused beam. Moreover, the signals were predicted to be equally strong for the two opposite-handed circular polarizations. As a consequence, THG-CD was absent from the disordered LD

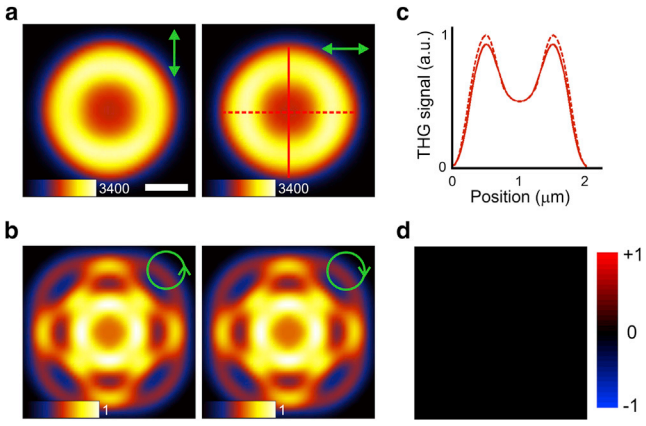

FIGURE 2 Simulated far-field THG intensity images of a 1.6-μm-diameter LD using tightly focused linear (*a*) and circular (*b*) polarizations under the same experimental parameters. The LD is assumed to be isotropic in 3D and the surrounding medium is water. The direction of the incident polarizations is shown by the arrow. Numbers at lower left indicate the maximum signal levels in each image. Scale bar, 500 nm. The solid and dashed lines in *a* represent the normalized line profile (*c*) acquired perpendicular and parallel, respectively, to the direction of the input linear polarization. (*d*) Calculated THG-CD image of the isotropic LD derived from the images in *b*. To see this figure in color, go online.

(Fig. 2 *d*), which agrees with our measurements for TAG LDs (Fig. 1 *c*).

THG imaging of LDs in intact mammalian cells

We then turned to polarization-dependent THG imaging of LDs in intact cells, using well-established murine macrophages (Raw 264.7 cells) as a model. We prepared macrophages with either TAG- or CE-enriched LDs by loading living cells with a fatty acid (oleic acid) or cholesterol, respectively (Fig. 3 *a*). Oleic acid loading results in a robust increase in TAG, with glyceryl trioleate representing the predominant species, whereas macrophage cholesterol loading results in CE storage, with cholesteryl oleate as a major species (29). Biochemical quantification of cellular neutral lipids demonstrated high purity and comparable lipid content in TAG- and CE-enriched LDs, enabling direct comparison of THG signals between samples (Fig. 3 *b*). We also verified the presence of LDs in the cells using brightfield and confocal laser scanning microscopy (Figs. S1 *a* and S2 in the Supporting Material). Of note, the neutral lipid dye LipidTOX green labeled TAG-enriched LDs more efficiently than CE-enriched ones (Fig. S1, *a* and *b*), probably due to the distinct physical properties of TAG- and CE-enriched LDs.

We performed scanning THG microscopy of macrophages with TAG- or CE-enriched LDs using the same imaging parameters as for synthetic LDs. Linear-polarization-dependent THG microscopy visualized intracellular LDs with an excellent signal/noise ratio (Fig. 3, *c*-*e*). Similar to the synthetic LDs, intracellular TAG-enriched LDs resulted in lower THG signal intensities compared to CE-enriched LDs (Fig. 3, *c*–*e*). Quantification of THG intensities for individual TAG- and CE-enriched LDs showed that the CE-enriched LDs had around sixfold higher mean and around tenfold higher maximum THG intensities. As THG signals are influenced by the size of the scatterer at a particular focusing condition (30), we quantified and compared the intensities of similar-sized LDs only. Furthermore, the excitation-spot size was always smaller than the LDs of interest, which per se abolishes size effects. The use of a small excitation-spot size is further indicated by the observation of doughnut-like intensity distributions in both experiments and simulations (Figs. 3, *d* and *e*, and 2 *a*). By inspection, the THG images of the TAG-enriched LDs (Fig. 3 *d*) agree qualitatively with the predictions for a disordered LD (Fig. 2 *a*). Although the corresponding THG images for the CE-enriched LDs are also doughnut-like, the resulting patterns appear less symmetrical (Fig. 3 *e*) than those for the TAG-enriched ones (Fig. 3 *d*). Taken together, the results from synthetic LDs, simulations, and experiments in cells imply that linear-polarization-dependent THG microscopy differentiates cellular TAG- and CE-enriched LDs due to their different ordering.

Our results with synthetic and simulated LDs provided evidence that THG microscopy with circular polarizations

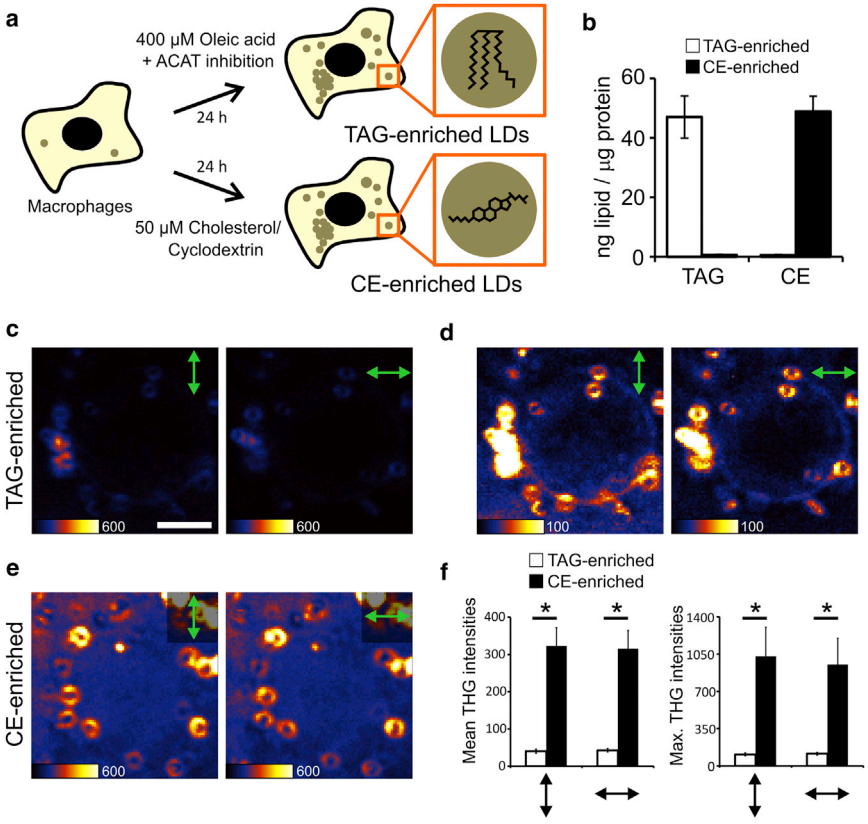

FIGURE 3 Generation and biochemical quantification of TAG- and CE-enriched LDs in cells, and THG imaging of cellular LDs under linear polarizations. (*a*) Raw 264.7 macrophages were treated with 400 μM oleic acid + 2 μg/mL Sandoz-58-035 (inhibitor for acyl-CoA:cholesterol acyltransferase 1 (*ACAT1*), the enzyme catalyzing fatty acid incorporation into CEs) or 50 μM cholesterol/cyclodextrin for 24 h for generation of TAG- or CE-enriched LDs, respectively. (*b*) Lipid quantification of macrophages with CE- and TAG-enriched LDs. The data are expressed as mean ± SE. Polarized THG microscopy of TAG- (*c* and *d*) and CE-enriched (*e*) LDs in cells using orthogonal linear polarizations at identical experimental settings. Scale bar, 5 μm. The same image is shown in *c* and *d*, but with different scales to facilitate comparison of TAG- and CE-enriched cells. Numbers at the lower left indicate the maximum signal level in each image. Arrows indicate the direction of incident linear polarization. See Fig. S2 for the corresponding brightfield images. (*f*) Quantification of the mean and maximum THG signals acquired from the TAG- and CE-enriched LDs under orthogonal linear polarizations. The data are from 22 TAG-enriched and 21 CE-enriched LDs and are expressed as the mean ± SE. $^*p \leq 0.05$. To see this figure in color, go online.

is also sensitive to intrinsic LD ordering. We therefore investigated cellular TAG- and CE-enriched LDs with circular polarizations (Fig. 4, *a–c*). Similar to the case for synthetic LDs, the signal intensities were much lower for left- and right-handed circular polarizations than for linear polarizations. Furthermore, the CE-enriched LDs showed a good signal/noise ratio, whereas the intensities for TAG-enriched LDs were close to the detection limit (Fig. 4, *a–c*). Quantification of similar-sized LDs revealed that CE-enriched LDs displayed around eightfold higher mean and around fivefold higher maximum intensities than TAG-enriched LDs (Fig. 4 *d*). Moreover, the THG images for opposite-handed circular polarizations exhibited higher signals for CE-enriched LDs (Fig. 4 *d*). Quantification of THG-CD for individual LDs showed that the normalized THG-CD signals of the CE-enriched LDs were about twice as high as those for the TAG-enriched LDs (Fig. 4 *e* and *f*). In fact, the THG-CD for TAG-enriched LDs is probably even lower than shown, because the absolute signals were already at the noise level. The differences in the normalized THG-CD values, together with the other results, strongly suggest that cellular CE-enriched LDs exhibit more pronounced intrinsic ordering than TAG-enriched LDs and that THG microscopy with circular polarizations can detect this.

Physiologically, cells can simultaneously store both TAG and CE, and based on fluorescent lipids, Raw 264.7 macrophages can deposit them in the same LDs (Fig. S3). To address the THG responses in such mixed LDs in macrophages, we induced LDs with variable TAG/CE ratios by coadministering different amounts of cholesterol and fatty acid (Fig. 5 and Fig. S4). Generally, we found an increasing trend in the THG signals with CE loading, and this trend is the same for linear and circular polarizations (Fig. 5, *b* and *c*, respectively). Nevertheless, for each sample, the signal levels for circular polarizations are much lower than for linear polarizations, as also observed for the samples discussed above. Note, however, that the THG signal growth does not scale linearly with the CE content. In particular, for both linear and circular polarizations, there is a significant change in the THG signals as the CE content increases from 41% to 52%. This threshold effect is particularly sharp for THG with circular polarizations, in agreement with the idea that the circular polarizations are a very direct indicator of ordering. These results suggest that upon incorporation of CE, the TAGs containing LDs initially remain disordered but with a further increase in their CE content, LDs undergo a transition to a more ordered state. This is in line with earlier observations that TAG depletion alters CE physical state in LDs (6).

CONCLUSION

Our findings show that polarized THG imaging can be used to discriminate cellular or synthetic LDs with different lipid composition due to their different intrinsic ordering effects. Both linear and circular polarizations can be used, but care must be exercised in interpreting the results for linear polarizations, as even disordered systems can lead to a dependence on linear polarization due to the

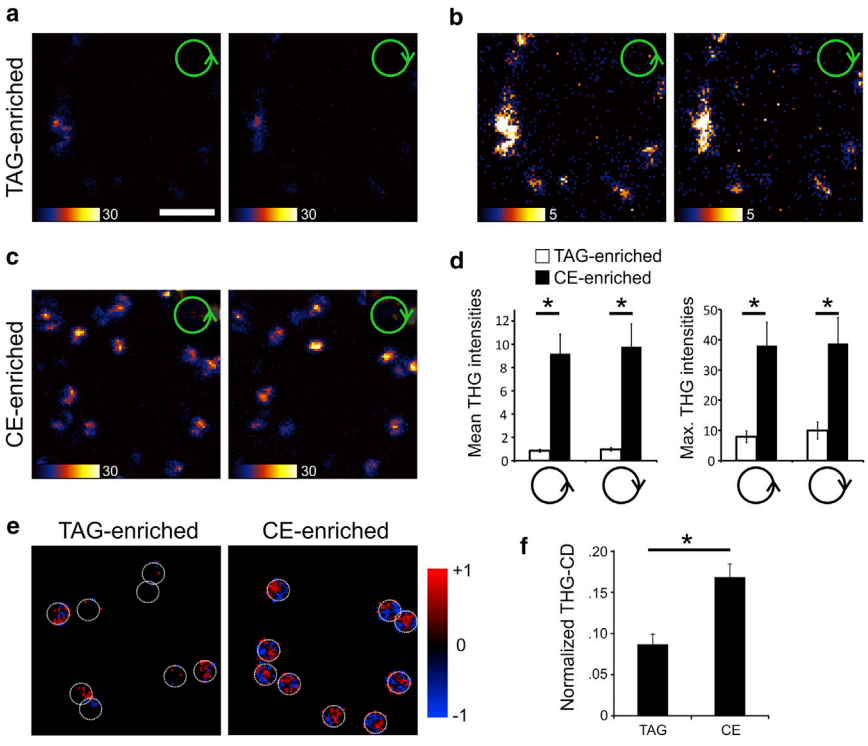

FIGURE 4 Polarized THG microscopy of TAG- (*a* and *b*) and CE-enriched (*c*) LDs in Raw 264.7 macrophages using opposite-handed circular polarizations at identical experimental settings. Scale bar, 5 μm. The same image is shown in *a* and *b*, but with different scales to facilitate comparison of TAG- and CE-enriched cells. Numbers at the lower left indicate the maximum signal levels in each image. Arrows indicate the direction of incident circular polarization. See Fig. S2 for the corresponding brightfield images. (*d*) Comparison of the mean and maximum THG signals acquired from the TAG- and CE-enriched LDs under left- and right-hand circular polarizations. The data are from 22 TAG-enriched and 21 CE-enriched LDs and are expressed as the mean ± SE. $*p \leq 0.05$. (*e*) Corresponding THG-CD microscopy images of TAG- and CE-enriched LDs in cells derived from the THG images using circular polarizations. Scale bar, 5 μm. (*f*) Normalized THG-CD of TAG- and CE-enriched LDs (mean ± SE, $n = 8$,$*p \leq 0.05$). White circles in *e* indicate the LDs of interest. For clarity, the spurious CD signals outside the highlighted regions are not shown. To see this figure in color, go online.

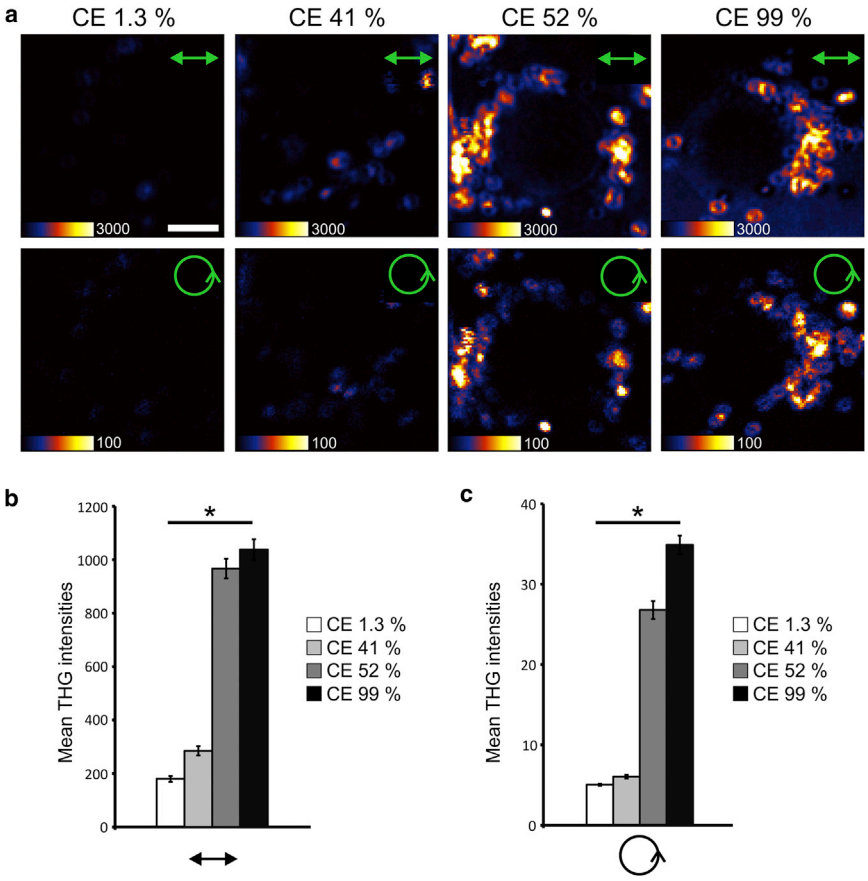

FIGURE 5 (*a*) Polarized THG microscopy of Raw 264.7 macrophage LDs with increasing fraction of CE relative to TAG. Cells were treated with 400 μM oleic acid (OA) + 2 μg/mL Sandoz-58-035 (1.3% CE), 35 μM cholesterol/cyclodextrin plus 400 μM OA (41% CE), 50 μM cholesterol/cyclodextrin + 400 μM OA (52% CE), or 50 μM cholesterol/cyclodextrin (99% CE) for 24 h, fixed, and subjected to THG microscopy using linear and circular polarizations. Scale bar, 5 μm. Lipid concentrations were determined from parallel cell samples (Fig. S4). (*b*) Comparison of the mean THG signals acquired from the LDs under linear polarization. (*c*) Comparison of the mean THG signals acquired from the LDs under circular polarization. The data in *b* and *c* are from individual LDs analyzed (1.3% CE, $n = 84$ LDs; 41% CE, $n = 68$; 52% CE, $n = 80$; 99% CE, $n = 73$) and are expressed as the mean $\pm$ SE. $^*p \leq 0.05$. To see this figure in color, go online.

properties of vectorial focused beams. As such, polarized THG microscopy provides to our knowledge the first label-free, spectroscopically nonresonant imaging method that differentiates between compositionally different LDs in intact mammalian cells. The use of tightly focused linear and circular polarizations and CD effects in THG microscopy provides a state-of-the-art optical technique for probing LD ordering and has potential for simple and clinically relevant diagnostics of lipid-related disorders.

SUPPORTING MATERIAL

Four figures and Supporting Methods are available at http://www.biophysj.org/biophysj/supplemental/S0006-3495(14)01060-1.

AUTHOR CONTRIBUTIONS

E.I. and M.K. conceptualized the problem. G.B. and M.J.H. designed and implemented the nonlinear imaging setup. G.B. performed the nonlinear experiments. S.G.P., S.R., and K.K. prepared the samples. S.G.P. performed the lipid analyses and confocal measurements. M.J.H. performed the modeling. All authors contributed to analysis of the data. G.B., S.G.P., E.I., and M.K. wrote the manuscript. All authors read and contributed to the writing of the manuscript.

The authors thank Biomedicum Imaging Unit, University of Helsinki, in particular A. Isomäki, for excellent core facility support and M. Grasso (Politecnico di Milano, Milan, Italy) for technical assistance.

This work was supported by Academy of Finland grants 134973 (to M.K.), 267847 (to G.B.), 275964 (to S.G.P.), 250081 (to K.K.), 135050 (to E.I.) and 263841 (to E.I.). S.G.P. received a personal fellowship from the Paulo Foundation. M.J.H. acknowledges support from the Graduate School of Modern Optics and Photonics in Finland and the Academy of Finland through its Centers of Excellence Programme (2012-2017) under project No. 251748 and by the European Research Council (ERC-2013-AdG-340748-CODE). This work is supported by Tampere University of Technology's Strategy Funding 2014 (84010). This work was performed in the context of the European COST Action MP1302 Nanospectroscopy.

The authors declare no competing financial interest.

SUPPORTING CITATIONS

References (31–34) appear in the Supporting Material.

REFERENCES

1. Martin, S., and R. G. Parton. 2006. Lipid droplets: a unified view of a dynamic organelle. *Nat. Rev. Mol. Cell Biol.* 7:373–378.
2. Moore, K. J., and I. Tabas. 2011. Macrophages in the pathogenesis of atherosclerosis. *Cell.* 145:341–355.
3. Daniel, J., H. Maamar, …, P. E. Kolattukudy. 2011. *Mycobacterium tuberculosis* uses host triacylglycerol to accumulate lipid droplets and acquires a dormancy-like phenotype in lipid-loaded macrophages. *PLoS Pathog.* 7:e1002093.
4. Xu, H., G. T. Barnes, …, H. Chen. 2003. Chronic inflammation in fat plays a crucial role in the development of obesity-related insulin resistance. *J. Clin. Invest.* 112:1821–1830.

5. Leroux, A., G. Ferrere, …, A. M. Cassard-Doulcier. 2012. Toxic lipids stored by Kupffer cells correlates with their pro-inflammatory phenotype at an early stage of steatohepatitis. *J. Hepatol.* 57:141–149.
6. Lada, A. T., M. C. Willingham, and R. W. St Clair. 2002. Triglyceride depletion in THP-1 cells alters cholesteryl ester physical state and cholesterol efflux. *J. Lipid Res.* 43:618–628.
7. Adelman, S. J., J. M. Glick, …, G. H. Rothblat. 1984. Lipid composition and physical state effects on cellular cholesteryl ester clearance. *J. Biol. Chem.* 259:13844–13850.
8. Engelman, D. M., and G. M. Hillman. 1976. Molecular organization of the cholesteryl ester droplets in the fatty streaks of human aorta. *J. Clin. Invest.* 58:997–1007.
9. Snow, J. W., H. M. McCloskey, …, M. C. Phillips. 1988. Physical state of cholesteryl esters deposited in cultured macrophages. *Biochemistry.* 27:3640–3646.
10. Small, D. M. 1988. George Lyman Duff memorial lecture. Progression and regression of atherosclerotic lesions. Insights from lipid physical biochemistry. *Arteriosclerosis.* 8:103–129.
11. Glick, J. M., S. J. Adelman, …, G. H. Rothblat. 1983. Cellular cholesteryl ester clearance. Relationship to the physical state of cholesteryl ester inclusions. *J. Biol. Chem.* 258:13425–13430.
12. Czabany, T., A. Wagner, …, G. Daum. 2008. Structural and biochemical properties of lipid particles from the yeast *Saccharomyces cerevisiae*. *J. Biol. Chem.* 283:17065–17074.
13. Evans, C. L., and X. S. Xie. 2008. Coherent anti-stokes Raman scattering microscopy: chemical imaging for biology and medicine. *Annu. Rev. Anal. Chem.* (*Palo Alto Calif).* 1:883–909.
14. Débarre, D., W. Supatto, …, E. Beaurepaire. 2006. Imaging lipid bodies in cells and tissues using third-harmonic generation microscopy. *Nat. Methods.* 3:47–53.
15. Suhalim, J. L., C. Y. Chung, …, E. O. Potma. 2012. Characterization of cholesterol crystals in atherosclerotic plaques using stimulated Raman scattering and second-harmonic generation microscopy. *Biophys. J.* 102:1988–1995.
16. Rinia, H. A., K. N. Burger, …, M. Müller. 2008. Quantitative label-free imaging of lipid composition and packing of individual cellular lipid droplets using multiplex CARS microscopy. *Biophys. J.* 95:4908–4914.
17. Müller, M., J. Squier, …, G. J. Brakenhoff. 1998. 3D microscopy of transparent objects using third-harmonic generation. *J. Microsc.* 191:266–274.
18. Zimmerley, M., P. Mahou, …, E. Beaurepaire. 2013. Probing ordered aipid assemblies with polarized third-harmonic-generation microscopy. *Phys. Rev. X.* 3:011002.
19. Oron, D., E. Tal, and Y. Silberberg. 2003. Depth-resolved multiphoton polarization microscopy by third-harmonic generation. *Opt. Lett.* 28:2315–2317.
20. Verbiest, T., M. Kauranen, …, A. Persoons. 1996. Optical activity of anisotropic achiral surfaces. *Phys. Rev. Lett.* 77:1456–1459.
21. Verbiest, T., S. V. Elshocht, …, A. Persoons. 1998. Strong enhancement of nonlinear optical properties through supramolecular chirality. *Science.* 282:913–915.
22. Wagnière, G. 1982. Optical activity of higher order in a medium of randomly oriented molecules. *J. Chem. Phys.* 77:2786–2792.
23. Bligh, E. G., and W. J. Dyer. 1959. A rapid method of total lipid extraction and purification. *Can. J. Biochem. Physiol.* 37:911–917.
24. Goldstein, J. L., S. K. Basu, and M. S. Brown. 1983. Receptor-mediated endocytosis of low-density lipoprotein in cultured cells. *Methods Enzymol.* 98:241–260.
25. Hölttä-Vuori, M., V. T. Salo, …, E. Ikonen. 2013. Alleviation of seipinopathy-related ER stress by triglyceride storage. *Hum. Mol. Genet.* 22:1157–1166.
26. Hsieh, K., Y. K. Lee, …, A. R. Kimmel. 2012. Perilipin family members preferentially sequester to either triacylglycerol-specific or cholesteryl-ester-specific intracellular lipid storage droplets. *J. Cell Sci.* 125:4067–4076.
27. Richards, B., and E. Wolf. 1959. Electromagnetic diffraction in optical systems. II. Structure of the image field in an aplanatic system. *Proc. R. Soc. Lond. A Math. Phys. Sci.* 253:358–379.
28. Cheng, J., and X. S. Xie. 2002. Green's function formulation for third-harmonic generation microscopy. *J. Opt. Soc. Am.* 19:1604–1610.
29. Bowden, J. A., F. Shao, …, D. A. Ford. 2011. Electrospray ionization tandem mass spectrometry of sodiated adducts of cholesteryl esters. *Lipids.* 46:1169–1179.
30. Débarre, D., W. Supatto, and E. Beaurepaire. 2005. Structure sensitivity in third-harmonic generation microscopy. *Opt. Lett.* 30:2134–2136.
31. Novotny, L., and B. Hecht. 2006. Principles of Nano-Optics. Cambridge University Press, Cambridge, United Kingdom.
32. Débarre, D., and E. Beaurepaire. 2007. Quantitative characterization of biological liquids for third-harmonic generation microscopy. *Biophys. J.* 92:603–612.
33. Kajzar, F., and J. Messier. 1985. Third-harmonic generation in liquids. *Phys. Rev. A.* 32:2352–2363.
34. Boyd, R. Nonlinear Optics. Academic Press, New York.